J Mol Model (2017) 23:54
DOI 10.1007/s00894-017-3230-2

ORIGINAL PAPER

Mechanism of extractive/oxidative desulfurization using the ionic liquid inimidazole acetate: a computational study

Hanlu Wang[1] · Mingsheng Xu[1] · Rujin Zhou[1]

Received: 18 August 2016 / Accepted: 12 January 2017

Abstract The dual role of the ionic liquid 1-butyl-3-methylimidazolium trifluoroacetic acid ([C_4mim]TFA) as an extractant for thiophene (TH) and a catalyst for the oxidation of TH was explored at the molecular level by performing density functional theory (DFT) calculations. The calculated interaction energies demonstrated why [C_4mim]TFA is a better extractant for thiophene sulfone (THO_2) than for TH. Two pathways were proposed for the oxidation of TH to THO_2 with [C_4mim]TFA acting as a catalyst. In the dominant pathway, a peracid is formed which then oxidizes TH to the sulfoxide and sulfones. The presence of [C_4mim]TFA was found to greatly reduce the barrier to the oxidative desulfurization (ODS) of TH using H_2O_2 as an oxidant.

Keywords Extraction/oxidation · Desulfurization · Imidazole acetate · Ionic liquid · DFT

Introduction

New and more stringent limits on the levels of sulfur permissible in fuel have been established in many countries [1, 2] because of environmental concerns about sulfur compounds, so the deep removal of these compounds from liquid fuels has attracted much attention. The traditional hydrodesulfurization process (HDS) is efficient at removing paraffinic sulfur compounds but inefficient at removing aromatic sulfides from fuels. Therefore, alternative desulfurization methods are urgently required for the production of ultra-low-sulfur fuels. Options include oxidative desulfurization (ODS), extractive desulfurization (EDS), biodesulfurization (BDS), among others [2]. However, each of these methods has disadvantages. That said, extractive/oxidative desulfurization shows great promise for industrial-scale applications as it requires little energy, mild operating conditions, and no hydrogen, and it retains the chemical structure of the fuel.

Ionic liquids (ILs) are low-melting organic salts that have attracted considerable attention due to their useful physicochemical properties, such as low vapor pressure, good thermal and chemical stability, designability, and reusability. These properties have led to the widespread use of ILs in chemical synthesis and extraction separation processes [3]. Many reports indicate that ILs can be applied in EDS methods because they are good at extracting aromatic sulfur compounds and are immiscible with aliphatic compounds [4–7]. Recently, ODS methods utilizing H_2O_2 or O_3 as the oxidant and an IL as both an extractant and catalyst have been developed [8–17]. The resulting extractive/oxidative desulfurization involves two steps: sulfur compounds are initially transformed into sulfones and sulfoxides by the oxidant, and these oxidized products are then removed by selective extraction with polar solvents [17].

Recently, computational methods have contributed greatly to our understanding of the interactions and reactions of ILs [18–30]. In the work reported in the present paper, we investigated the mechanism for the extractive/oxidative desulfurization of thiophene (TH) in the presence of the ionic liquid [C_4mim]TFA, which is reported to be a good extractant and

---

Electronic supplementary material The online version of this article (doi:10.1007/s00894-017-3230-2) contains supplementary material, which is available to authorized users.

✉ Hanlu Wang
wanghlu@mail2.sysu.edu.cn

✉ Rujin Zhou
rujinzhou@126.com

[1] College of Chemical Engineering, Guangdong University of Petrochemical Technology, Maoming 525000, People's Republic of China

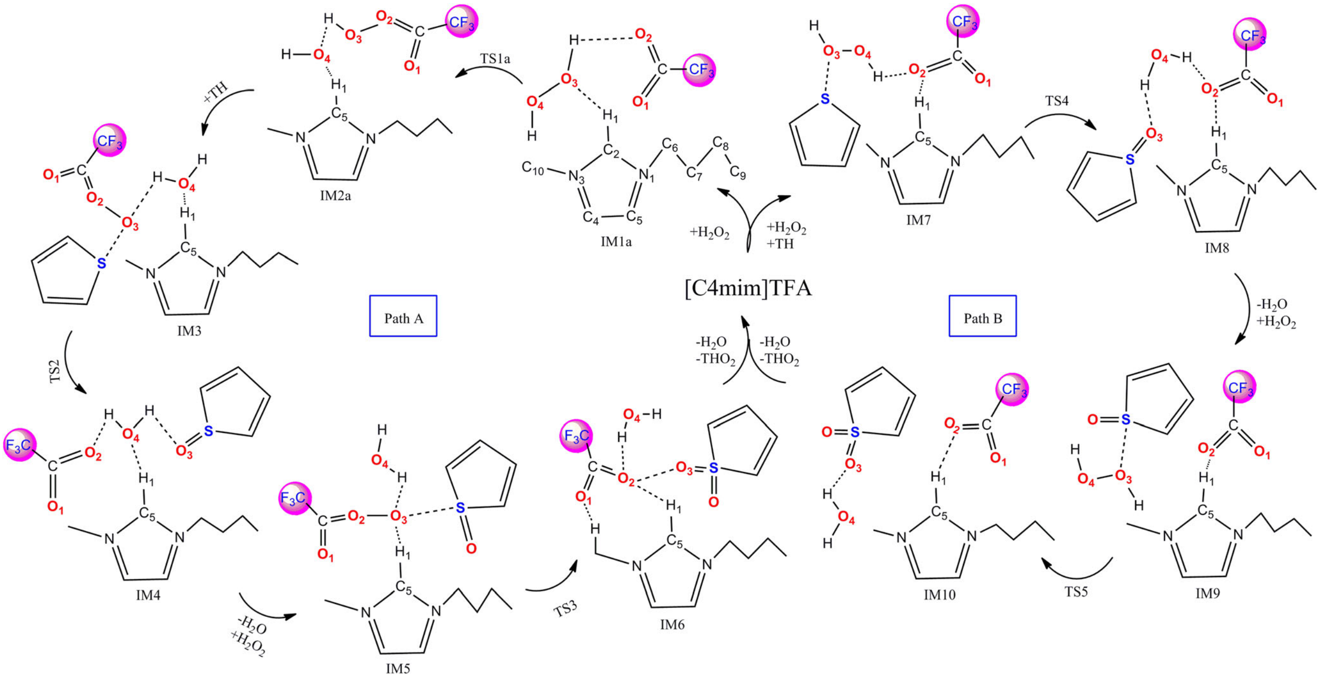

Fig. 1 Two possible mechanisms for the oxidation of TH catalyzed by $[C_4mim]TFA$

catalyst for ODS of model oil using H_2O_2 as an oxidant [17]. We therefore performed an in-depth study of the mechanism for the oxidation of thiophene (TH) into thiophene sulfone (THO_2) by H_2O_2, as catalyzed by $[C_4mim]TFA$ (Fig. 1), and explored the dual role of $[C_4mim]TFA$ as an extractant and catalyst in the extractive/oxidative desulfurization process.

Methods

It is well known that density functional theory (DFT) methods offer an excellent compromise between computational cost and the accuracy of the results of the computations. Therefore, we performed DFT calculations at the B3LYP/6-311++G(d, p) level of theory in this work [31, 32]. All of the structures of the reactants, products, intermediates, and transition states were fully optimized without any symmetry constraints. Vibrational frequencies were also calculated for all optimized geometries at the same level of theory to identify the nature of each stationary point as either a minimum (no imaginary vibrations) or a transition state (one imaginary vibration). Intrinsic reaction coordinate (IRC) calculations [33, 34] were performed in both directions (forward and reverse) from transition states to the corresponding local minima to identify the minimum-energy paths (Figs. S1–S5 in the "Electronic supplementary material," ESM). Moreover, single-point energies were calculated at the same level with D3 corrections, as these describe weak interactions well and have proven to be accurate in a variety of simulations [30, 35–37]. The relative free energies with and without D3 for different paths are listed in Tables 1, 2, and 3. Electrostatic analysis and natural bond orbital (NBO) charge analysis [38] were performed to elucidate the bonding and chemical reactivity. Frontier molecular orbitals were obtained by single-point calculations based on the optimized geometries using B2PLYPD/6-311++G(d,p) [39, 40]. All calculations were carried out with the Gaussian09 software package [41].

Since accurate structures are a prequisite for studying a reaction, it was important to choose a model that can generate reasonable structures for the title compounds. As shown in Fig. 2, when compared with the experimental data for the S—C bonds in the compounds of interest (1.71 Å in TH and 1.80 Å in THO and THO_2), we found that the calculated bond lengths (1.733 Å for TH) were slightly longer [42]. The minor differences between the experimental and the calculated S—C bond lengths can be ascribed to systematic errors associated

Table 1 Comparison of the relative free energies (kcal mol^{-1}) for the superoxidation of IL by H_2O_2 along path A, with and without D3 correction

	IL-I+H_2O_2	IM1a	TS1a	IM2a	IM1b	TS1b	IM2b	IM1c	TS1c	IM2c
B3LYP	0.0	−1.1	35.9	17.5	−2.4	41.7	18.7	−2.9	41.5	8.7
B3LYP+D3	0.0	−5.8	31.0	13.9	−6.0	37.8	14.1	−8.6	35.8	5.8

Table 2 Comparison of the relative free energies (kcal mol^{-1}) for the formation of the sulfoxide (THO) and sulfone (THO_2) of TH along path A, with and without D3 correction

	IM2a+TH	IM3	TS2	IM4	IM5	TS3	IM6
B3LYP	0.0	6.3	22.8	−26.8	−11.1	−0.9	−73.8
B3LYP+D3	0.0	0.0	12.7	−32.5	−19.0	−9.2	−82.5

Table 3 Comparison of the relative free energies (kcal mol^{-1}) for the formation of the sulfoxide (THO) and sulfone (THO_2) of TH along path B, with and without D3 correction

	IL-I+H_2O_2+TH	IM7	TS4	IM8	IM9	TS5	IM10
B3LYP	0.0	5.4	46.4	−8.3	−11.9	14.4	−68.4
B3LYP+D3	0.0	−4.9	33.4	−21.8	−11.0	13.7	−68.4

with the computational method/basis set employed as well as environmental factors. Consequently, the computations performed here can be considered to be reliable.

Results and discussion

Conformation of [C4mim]TFA

The geometry of [C4mim]TFA was optimized in order to understand its internal interactions before assigning its initial geometry. Three different initial conformations (I, II, III) were considered for [C4mim]TFA, and the most stable geometries were identified by determining the lowest-energy conformers. The main difference between these conformations was the orientations of the H-bonds that formed between [C4mim]$^+$ and TFA$^-$. As shown in Fig. 3, conformer I (IL-1) is the most stable conformer based on the relative energies. In this conformer, the H atoms at C2 and C6 form two strong H-bonds with O1 and O2 in TFA, respectively. In conformer II (IL-II), the H atoms at C5 and C6 form H-bonds with O1 and O2, respectively. In conformer III (IL-III), the H atoms at C4 and C10 form H-bonds with O1 and O2, respectively. The relative energies of IL-II and IL-III are much higher (by 8.4 and 9.0 kcal mol^{-1}, respectively) than that of IL-I. Therefore, IL-I was adopted for subsequent investigations.

Frontier molecular orbital and NBO charge analysis

As shown in Fig. 4, we investigated the highest occupied molecular orbital (HOMO) of the electron donor and the lowest unoccupied molecular orbital (LUMO) of the electron acceptor as well as the HOMO–LUMO energy gap ($\Delta\varepsilon$) in order to explore H-bonding and stability, which help to determine the mechanism of extractive/oxidative desulfurization. The HOMO of the isolated TFA$^-$ mainly comprises two $\pi_{C=O}$ bond orbitals, whereas the LUMO of the isolated cation [C4mim]$^+$ is the anti-π (π*) bond orbital, which does not readily accept an electron from the anion. In the IL, the anion dominates the IL's HOMO and tends to participate in H-bonds. A larger $\Delta\varepsilon$ value for a molecule implies higher stability. The corresponding $\Delta\varepsilon$ values of IL-I, IL-II, and IL-III are 8.02, 7.30, and 7.33 eV, respectively, again indicating that IL-I is the most stable conformer. Figure 5 depicts the electrostatic potentials of the sulfides and IL conformers. TH and THO have positive regions of electrostatic potential around the C–S bonds, in accordance with [43, 44]. These regions attract negatively charged sites on other species, such as oxygens in the peracid ([C4min]CF_3COOO^-). Electrostatic attraction

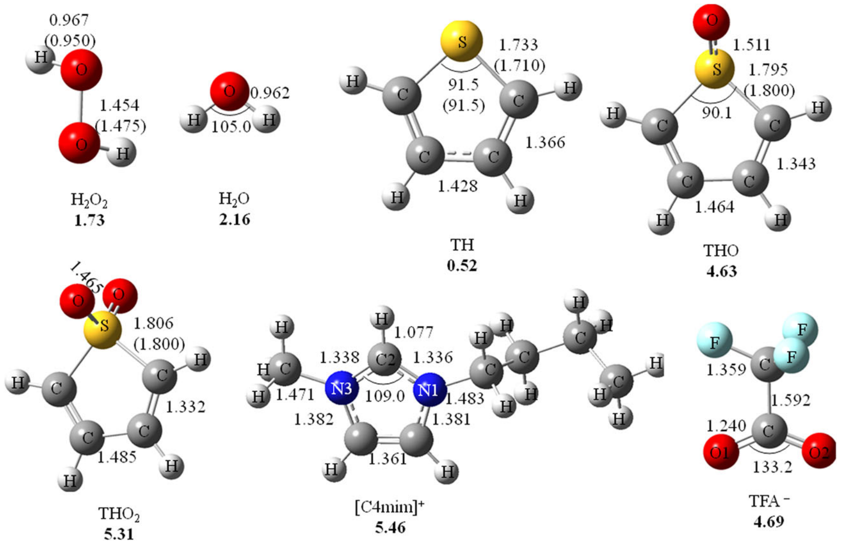

Fig. 2 Optimized geometries calculated at the B3LYP/6-311++G(d,p) level for the isolated molecules. Bond distances are in angstroms and angles are in degrees. *Values in parentheses* are experimental results and *bold values* are dipole moments (in D)

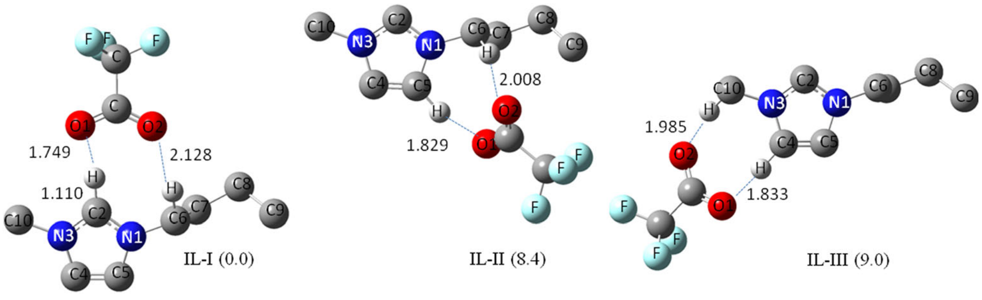

Fig. 3 Conformations and relative energies (kcal mol^{-1}) of [C4mim]TFA. Distances are in Å. Some H atoms have been omitted for clarity

drives the anion to approach the cation and to localize at the most positively charged region on the cation. To acquire more information in this context, NBO charges were calculated for [C4mim]$^+$, TFA$^-$, and the three conformers of the IL, as shown in Table 4. The charges on O1 and O2 in TFA$^-$ are negative so these oxygens act as potential electron acceptors. C2 and all of the H atoms in [C4mim]$^+$ are positively charged, with C2 exhibiting the highest positive charge (0.295). According to the data shown in Table 4, the H-bonds that form within IL-I (C2–H…O1, C6–H…O2) are the strongest among the three conformers.

Extraction mechanism

Elucidating the extraction mechanism is crucial to understanding the EDS process, which is important when attempting to design effective IL extractants. When TH is extracted into the IL phase, it is oxidized by the IL and H_2O_2 to produce THO_2, which remains in the IL phase because its polarity is similar to that of the IL. The extraction equilibrium is therefore disturbed, resulting in the continuous extraction of TH from the fuel into the IL phase until no more TH remains in the fuel [8–17]. In order to explore this extraction mechanism further, the interactions between the IL and sulfides were investigated in detail.

Figure 6 shows the most stable structures of the complexes of IL-I, [C4mim]$^+$, and TFA$^-$ with TH and THO_2. IL-I interacts with TH through a weak H-bond: C–H…C(TH). [C4mim]$^+$ interacts with TH through two H-bonds: C–H…C (3.026 Å) and N–H…S (2.836 Å). TFA$^-$ interacts with TH through the two H-bonds C–H…F (2.941 Å) and C–H…O (2.037 Å). The interaction energies between IL-I and sulfides play an important role in the extraction of sulfides from the fuel. The calculated interaction energies for these three complexes (i.e., IL-I, [C4mim]$^+$, and TFA$^-$ with TH) are −4.5, −5.1, and −7.2 kcal mol^{-1}, respectively, indicating that the ability to capture TH increases in the order IL-I < [C4mim]$^+$ < TFA$^-$. This suggests that the anion plays the most important role in the extraction and separation of TH.

IL-I interacts with THO_2 through a single H-bond, C–H…O (2.368 Å). [C4mim]$^+$ interacts with THO_2 through two H-bonds: C–H…O (2.320 and 2.063 Å, respectively). TFA$^-$ interacts with TH through the H-bonds C–H…O (2.222 Å) and C–H…F (2.621 Å). The calculated interaction energies for these three complexes (i.e., IL-I, [C4mim]$^+$, and TFA$^-$ with THO_2) are −12.8, −16.7, and −17.0 kcal mol^{-1}, respectively,

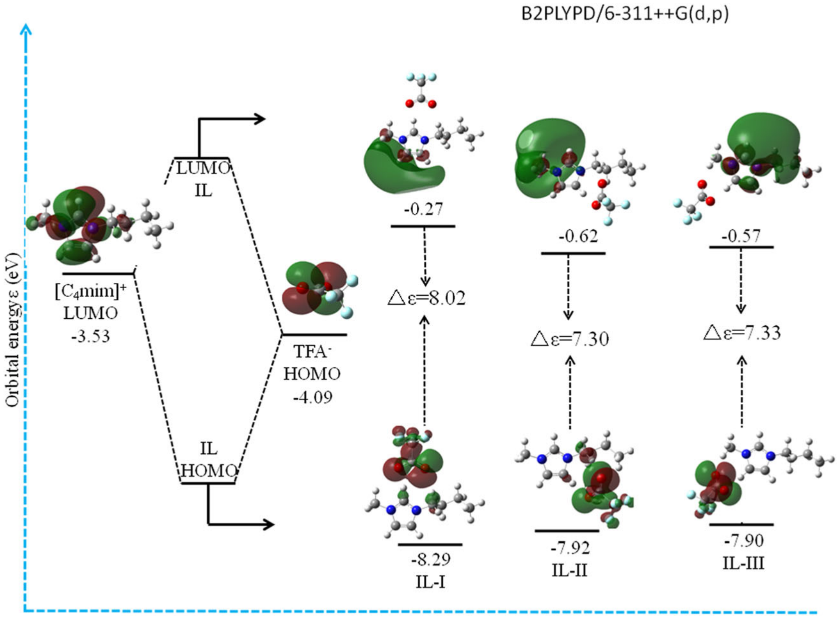

Fig. 4 Orbital diagrams for the three IL conformers when the TFA$^-$ approaches [C4mim]$^+$

Fig. 5 Electrostatic potentials of the sulfides and the IL conformations. *Red* signifies negative charge and *blue* corresponds to positive charge

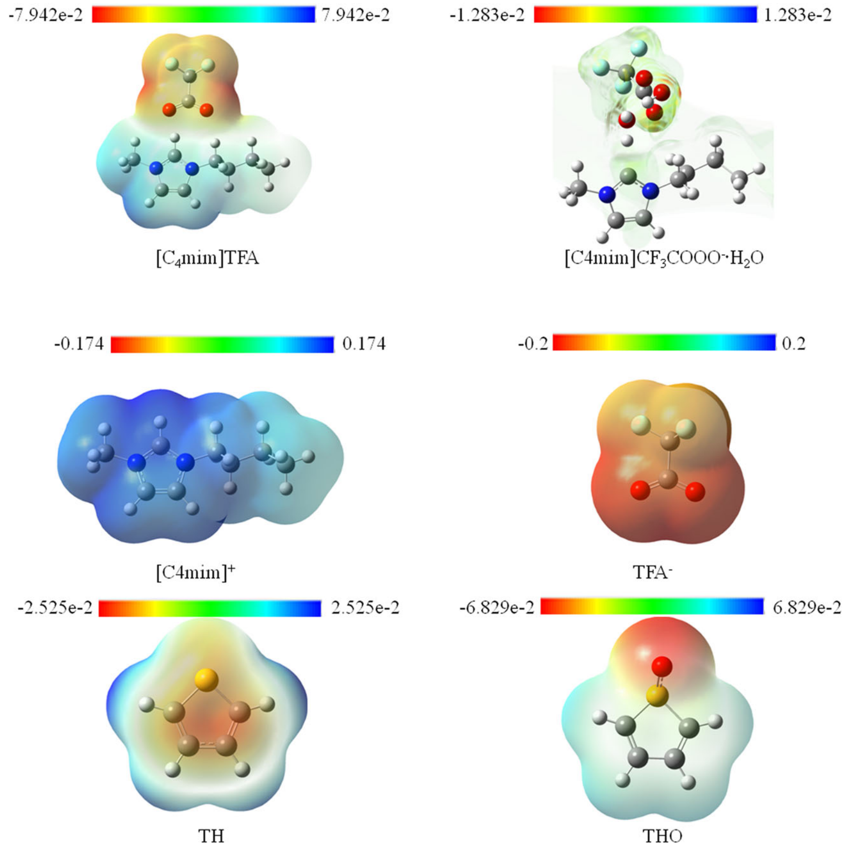

$[C_4mim]TFA$ $[C4mim]CF_3COOO^-H_2O$ $[C4mim]^+$ TFA^- TH THO

indicating that the ability to capture THO_2 increases in the order IL-I < $[C4mim]^+$ ≈ TFA^-. This indicates that both the cation and anion play important roles in the extraction and separation of THO_2.

The calculated interaction energies with THO_2 are clearly much larger than those with TH, indicating that IL-I is better at capturing THO_2 than it is at capturing TH. As depicted in Fig. 2, TH was found to be a nonpolar molecule, with a dipole moment of only 0.52 D. In contrast, THO_2 was found to be a highly polar molecule, with a dipole moment of 5.31 D. Hence, THO_2 prefers to remain in the (polar) IL phase, as has been demonstrated by Xu et al. [22].

Table 4 NBO charges of the isolated cation and anion and the three conformations of [C4mim]TFA (values are in |*e*|)

Atom	$[C4mim]^+$	TFA^-	IL-I	IL-II	IL-III
N1	−0.343		−0.358	−0.339	−0.361
N3	−0.347		−0.365	−0.363	−0.338
C2	0.295		0.298	0.271	0.268
C4	−0.007		−0.035	−0.042	0.002
C5	−0.003		−0.024	0.004	−0.039
H1	0.237		0.293	0.220	0.219
H2	0.223		0.279	0.290	0.212
H3	0.247		0.229	0.303	0.230
H4	0.247		0.227	0.231	0.302
H5	0.228		0.251	0.217	0.292
O1		−0.738	−0.756	−0.744	−0.745
O2		−0.738	−0.734	−0.739	−0.739

Oxidation of TH by [C4mim]TFA

After being extracted into the IL phase, TH is expected to undergo oxidation by the IL and H_2O_2 to form THO_2 (i.e., an initial oxidation to THO followed by a further oxidation to THO_2 [17]).

There are two possible pathways, A and B, for the oxidation of TH, as shown in Fig. 1. The main difference between the pathways is the oxidation sequence. The geometries of the transition states involved in these pathways are presented in Fig. 7, while the intermediates and products are depicted in Figs. 8, 9, and 10. Figure 11 shows the relevant energy profiles.

In pathway A, [C4min]TFA is first oxidized to the peracid ($[C4min]CF_3COOO^-$) by H_2O_2, and then the polarized TH is oxidized to THO and THO_2 by the peracid. For a catalytic reaction, the binding of the substrate to the catalyst is an essential initial step. The interaction of the IL with H_2O_2 is expected to be stronger than its interaction with TH, leading to stronger H-bonds between the IL and H_2O_2. Upon optimizing the structure of the complex between the IL and H_2O_2, three stable geometries (IM1a, IM1b, and IM1c) were

Fig. 6 Optimized geometries of the complexes of TH and THO_2 with IL-I, $[C4mim]^+$, and TFA^-. Distances are in Å. *Values in square brackets* are calculated interaction energies (kcal mol^{-1}). Some H atoms have been omitted for clarity

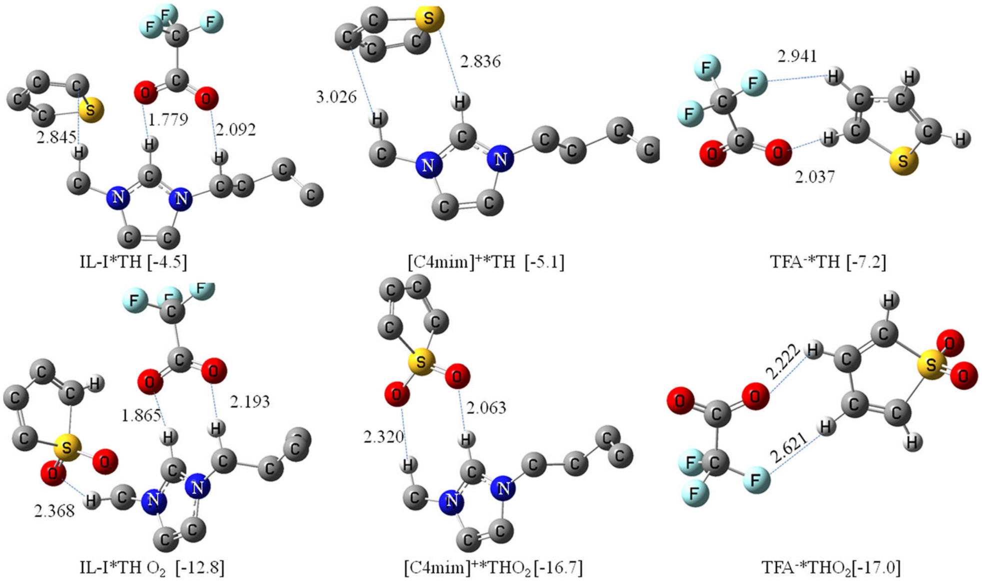

IL-I*TH [-4.5]

$[C4mim]^+$*TH [-5.1]

TFA^-*TH [-7.2]

IL-I*TH O_2 [-12.8]

$[C4mim]^+$*THO_2[-16.7]

TFA^-*THO_2[-17.0]

obtained, as shown in Fig. 8. The widely accepted mechanism for ODS using organic acids as catalysts involves the formation of a peracid in a reaction between a carboxylic acid and H_2O_2 [45]. Starting from these three structures, three possible channels for the oxidation of [C4min]TFA to the peracid ($[C4mim]CF_3COOO^- \cdot H_2O$) were explored: channels a, b, and c, which start from the structures IM1a, IM1b, and IM1c, respectively. In IM1a, O2 of TFA^- forms a H-bond with a H of H_2O_2. In IM1b, O2 of TFA^- forms H-bonds with both a H of H_2O_2 and H(C2) of $[C4mim]^+$. In IM1c, the O atoms of TFA^- form H-bonds with a H of H_2O_2 and H(C2) of $[C4mim]^+$. Three transition states (TS1a, TS1b, and TS1c) are thus obtained in which the O3–O4 bond in H_2O_2 is breaking and an O3–O2 bond is forming. Among these paths, path a exhibits the lowest barrier, 36.8 kcal mol^{-1}, and is endothermic by 19.7 kcal mol^{-1}. The resulting peracid IM2a oxidizes TH to THO_2 (while IM2a is simultaneously reduced). The water produced in this oxidation remains in the system, leading to local partial solvation.

Pathway A for the oxidation of TH with the IL acting as a catalyst is depicted in Fig. 9. When TH closely approaches IM2a, IM3 is formed, which has almost exactly the same energy as the isolated reactants (IM2a, TH). IM3 overcomes a barrier of 12.7 kcal mol^{-1} and passes through the transition state TS2, with vibrational data clearly indicating that this involves the rupture of the O2–O3 bond and the simultaneous

Fig. 7 Optimized structures of the transition states involved in the oxidation of TH by H_2O_2 with the aid of IL-I. Distances are in Å. Some H atoms have been omitted for clarity

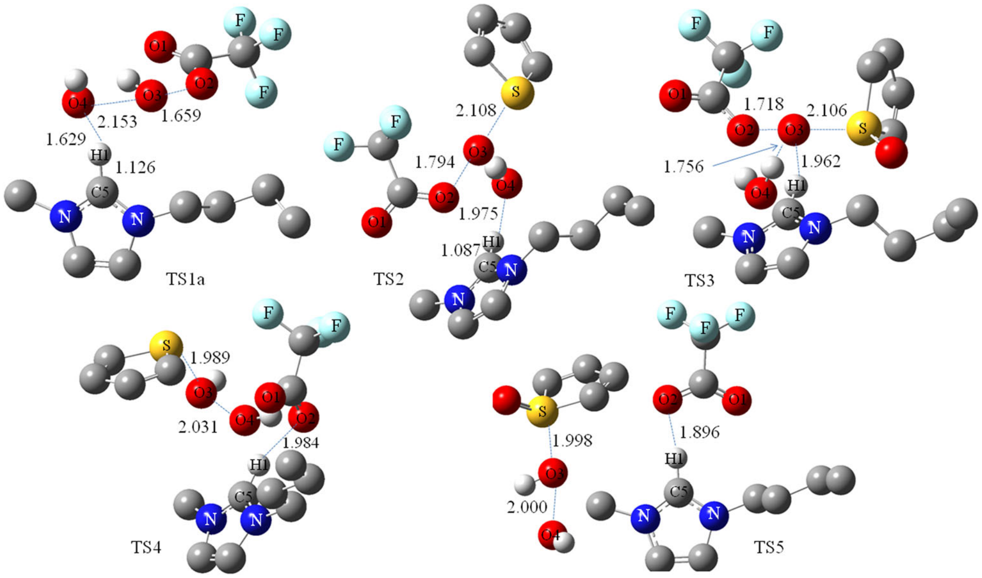

TS1a

TS2

TS3

TS4

TS5

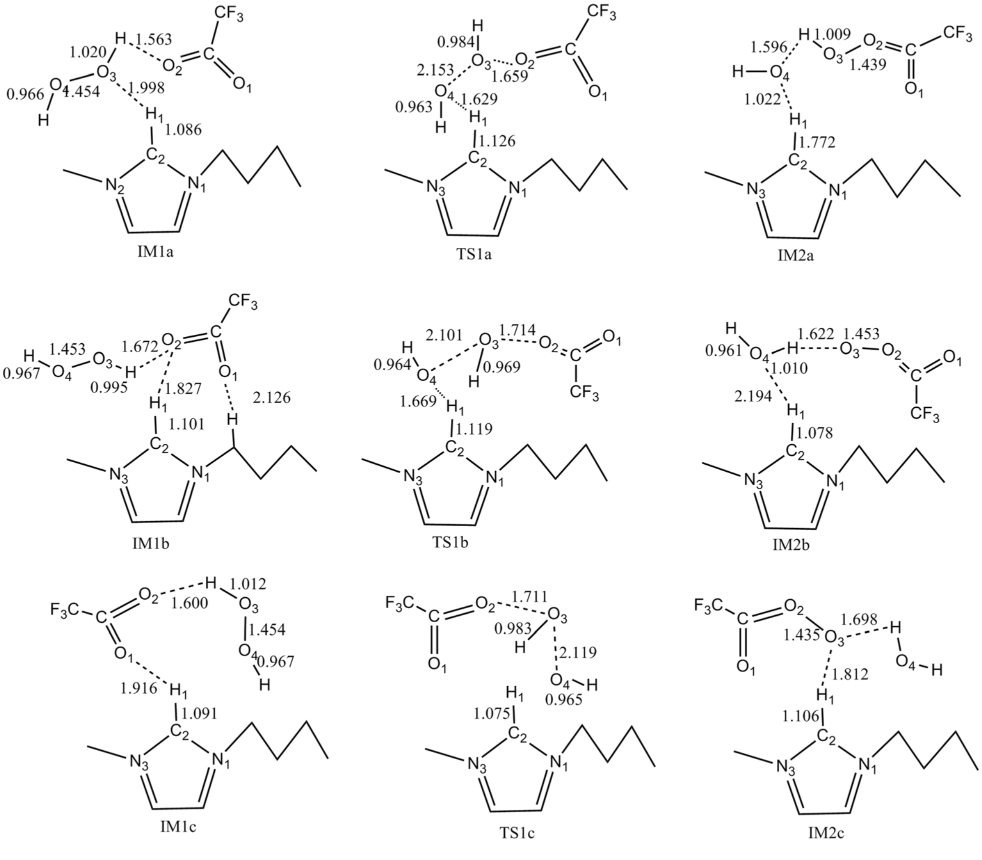

Fig. 8 Optimized structures and selected structural parameters for the three possible channels for the initial oxidation of the IL to the peracid in pathway A

formation of an O3–S bond. In the resulting IM4, the TH transforms into the sulfoxide (THO) and the water molecule forms a H-bond with the H atom at C2. This step is exothermic by 32.5 kcal mol^{-1}. In the subsequent oxidation process, H_2O is removed and H_2O_2 is added to IM4 to form IM5 in a process that is endothermic by 13.5 kcal mol^{-1}. The structure of TS3 is very similar to that of TS2, and its generation involves the cleavage of O2–O3 and the formation of an O3–S bond. The computed barrier to TS3 is only 9.8 kcal mol^{-1}, and this step is highly exothermic (by 63.5 kcal mol^{-1}). Finally, the stable

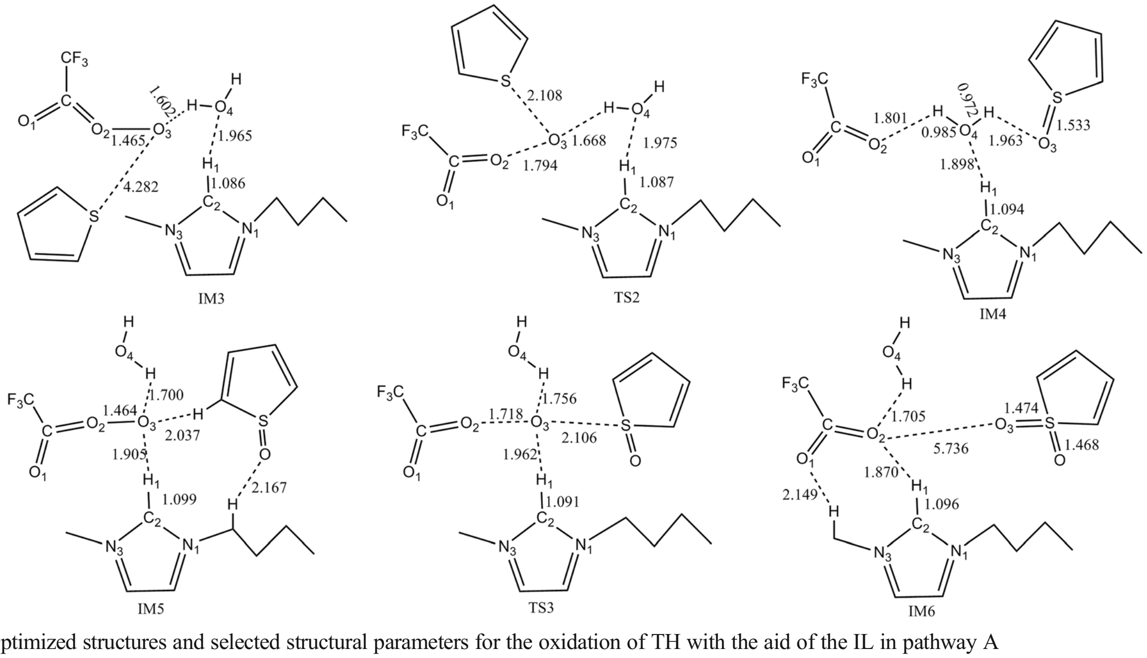

Fig. 9 Optimized structures and selected structural parameters for the oxidation of TH with the aid of the IL in pathway A

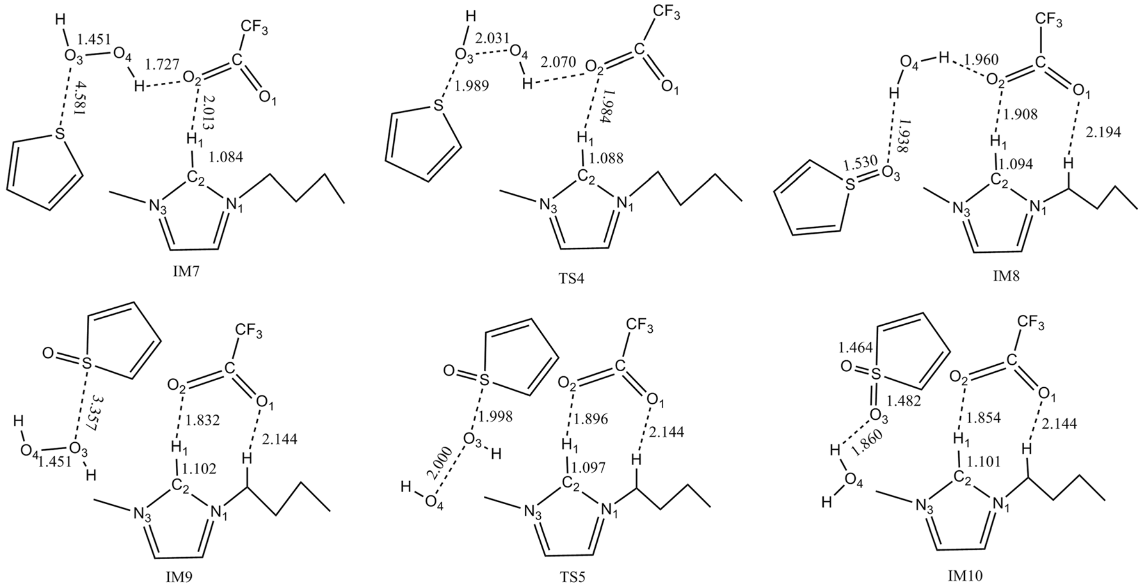

Fig. 10 Optimized structures and selected structural parameters for the oxidation of TH with the aid of the IL in pathway B

sulfone THO_2 (IM6) is formed, indicating that this reaction happens very quickly and is irreversible. In path A, the rate-determining step is peracid formation, with an activation barrier of 36.8 kcal mol^{-1}.

In pathway B, TH is directly oxidized to THO_2 by H_2O_2, with the IL acting as a spectator. This involves a mechanism qualitatively similar to the reaction in the absence of the IL, i.e., it involves two main steps: TH is oxidized first to THO and then to THO_2 [22, 46]. As shown in Fig. 10, IM7 in pathway B is a three-molecule complex of the IL, H_2O_2, and TH formed via H-bonds and van der Waals interactions; it is 4.9 kcal mol^{-1} more stable than the isolated reactants (IL, H_2O_2, and TH). Along the reaction coordinate, TH in IM7 is oxidized to THO through TS4, which has a barrier of 38.3 kcal mol^{-1} and is exothermic by 16.9 kcal mol^{-1}. In TS4, the nucleophilic O3 atom in H_2O_2 directly attacks the electron-deficient S atom in TH to produce THO; the O3–O4 bond breaks at the same

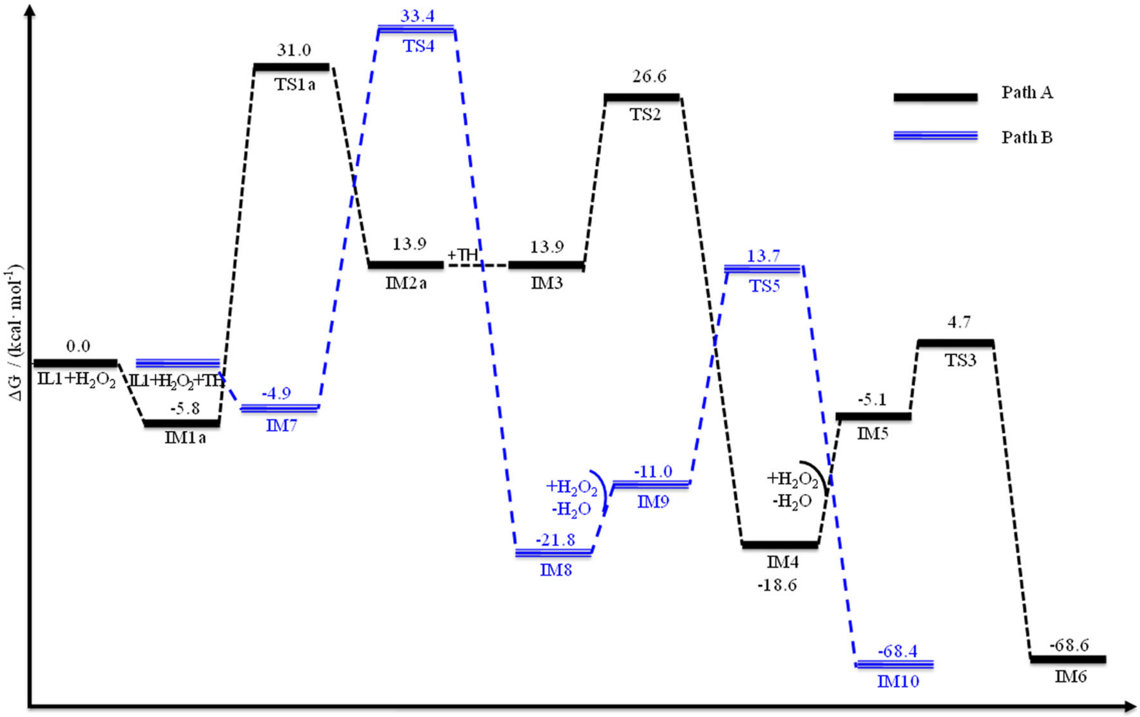

Fig. 11 Free-energy profiles for the oxidation of TH by H_2O_2 with the aid of IL-I via pathways A and B, as calculated at the B3LYP-D3/6-311++G(d, p) level

time. Then, after removing a H_2O, another H_2O_2 is introduced into IM8 to form IM9, a three-molecule complex of IL, H_2O_2, and THO. The THO in IM9 is further oxidized to THO_2 via TS5, which has a barrier of 13.7 kcal mol^{-1} and a reaction heat of 57.4 kcal mol^{-1}, indicating that the formation of THO_2 is an irreversible process. In TS5, the O3–O4 bond is breaking and a S–O3 bond is forming. For path B, the rate-determining step is expected to be THO formation, with a barrier of 38.3 kcal mol^{-1}.

As shown in Fig. 11, the calculated results indicate that pathway A is more energetically favorable than pathway B. Consequently, path A dominates in the reaction mechanism for ODS in the presence of the IL. The activation barrier for the reaction (TH + H_2O_2) in the absence of the IL was calculated by Zeng et al. to be 50.5 kcal mol^{-1} [46], i.e., much higher than that with IL (36.8 kcal mol^{-1}). This indicates that the IL plays an important role—it stabilizes all of the species involved in the reaction, especially the transition states, through ion–molecule H-bonds.

Conclusions

In summary, the reaction mechanism for the extractive/oxidative desulfurization of TH by [C_4mim]TFA in the presence of H_2O_2 was explored by performing DFT calculations.

Both the cation and the anion of the IL show stronger interactions with THO_2 than with TH, which can be attributed to the greater polarity of THO_2 than TH. The calculated interaction energies of the cation–sulfone complexes were also found to be similar to those of the anion–sulfone complexes, indicating that both the cation and the anion play important roles in the extraction and separation of aromatic sulfur compounds from fuels. On the other hand, in the oxidative reaction, it was predicted that TFA$^-$ is first oxidized to a peracid ([C4min]CF_3COOO^-) by H_2O_2, and then TH is oxidized to the sulfoxide and sulfones by the peracid. The introduction of [C4mim]TFA into the reaction system lowers the barrier to the ODS of TH using H_2O_2 as an oxidant from 50.5 kcal mol^{-1} to 36.8 kcal mol^{-1}. The present results thus provide insight into the mechanism of extractive/oxidative desulfurization by acidic ionic liquids in the presence of H_2O_2.

Acknowledgements This work was financially supported by the National Natural Science Foundation of China (21403038), the Guangdong Provincial Natural Science Foundation (2015A030313892), the Training Program for Outstanding Young Teachers in Colleges and Universities in Guangdong Province (YQ2015116), and the Students Innovation and Entrepreneurship Training Program in Guangdong University of Petrochemical Technology (201511656006).

References

1. Tian Y, Yao Y, Zhi Y, Yan L, Lu S (2015) Energy Fuel 29: 618–625
2. Zhao H, Baker G (2015) Front Chem Sci Eng 9(3):262–279
3. Amarasekara AS (2016) Chem Rev 116(10):6133–6183
4. Yao T, Yao S, Pan C, Dai X, Song H (2016) Energy Fuel 30(6): 4740–4749
5. Safa M, Mokhtarani B, Mortaheb HR (2016) Chem Eng Res Des 111:323–331
6. Kianpour E, Azizian S, Yarie M, Zolfigol MA, Bayat M (2016) Chem Eng J 295:500–508
7. Dharaskar SA, Wasewar KL, Varma MN, Shende DZ (2016) Environ Sci Pollut Res 23(10):9284–9294
8. Jiang B, Yang H, Zhang L, Zhang R, Sun Y, Huang Y (2016) Chem Eng J 283:89–96
9. Doherty S, Knight JG, Carroll MA, Clemmet AR, Ellison JR, Backhouse T, Holmes N, Thompson LA, Bourne RA (2016) RSC Adv 6(77):73118–73131
10. Zheng D, Zhu W, Xun S, Zhou M, Zhang M, Jiang W, Qin Y, Li H (2015) Fuel 159:446–453
11. Wu J, Gao Y, Zhang W, Tan Y, Tang A, Men Y, Tang B (2015) Appl Organomet Chem 29(2):96–100
12. Julião D, Gomes AC, Pillinger M, Cunha-Silva L, de Castro B, Gonçalves IS, Balula SS (2015) Fuel Process Technol 131:78–86
13. Chen X, Guo H, Abdeltawab AA, Guan Y, Al-Deyab SS, Yu G, Yu L (2015) Energy Fuel 29(5):2998–3003
14. Zhou M, Meng W, Li Y, Wang Q, Li X, Zang S (2014) Energy Fuel 28(1):516–521
15. Wu J, Gao Y, Zhang W, Tan Y, Tang A, Men Y, Tang B (2014) RSC Adv 4:58800–58804
16. Ma C, Dai B, Liu P, Zhou N, Shi A, Ban L, Chen H (2014) J Ind Eng Chem 20(5):2769–2774
17. Fang D, Wang Q, Liu Y, Xia L, Zang S (2014) Energy Fuels 28: 6677–6682
18. Zhou X, Cao B, Liu S, Sun X, Zhu X, Fu H (2016) J Mol Model 22(6):1–11
19. Song Z, Zhang J, Zeng Q, Cheng H, Chen L, Qi Z (2016) Fluid Phase Equilib 425:244–251
20. Oliveira OV, Paluch AS, Costa LT (2016) Fuel 175:225–231
21. Li H, Zhu W, Zhu S, Xia J (2016) AIChE J 62(6):2087–2100
22. Xu H, Han Z, Zhang D, Liu C (2015) J Mole Catal A Chem 398: 297–303
23. Vafaeezadeh M, Aboudia J, Hashemib MM (2015) RSC Adv 5: 58005–58009
24. Thomas E, Vijayalakshmi KP, George BK (2015) RSC Adv 5: 71896–71902
25. Rezabal E, Schäfer T (2015) Phys Chem Chem Phys 17:14588–14597
26. Ludwig R (2015) Phys Chem Chem Phys 17:13790–13793
27. Garcıa G, Atilhanb M, Aparicio S (2015) Phys Chem Chem Phys 17:16315–16326
28. Pilli SR, Banerjee T, Mohanty K (2015) J Mol Liq 207:112–124
29. Silva CM, Silva PL, Pliego JR (2014) Int J Quantum Chem 114(8): 501–507
30. Martins MJF, Ferreira AR, Konstantinova E, de Abreu HA, Souza WF, Chiaro SSX, Dias LG, Leitão AA (2012) Int J Quantum Chem 112(19):3234–3239
31. Becke AD (1993) J Chem Phys 98:5648–5652
32. Lee C, Yang W, Parr RG (1988) Phys Rev B 37:785–789
33. Gonzalez C, Schlegel HB (1990) J Phys Chem 94:5523–5527
34. Gonzalez C, Schlegel HB (1989) J Chem Phys 90(4):2154–2161

35. Van Speybroeck V, Van der Mynsbrugge J, Vandichel M, Hemelsoet K, Lesthaeghe D, Ghysels A, Marin GB, Waroquier M (2011) J Am Chem Soc 133(4):888–899
36. Grimme S, Antony J, Ehrlich S, Krieg H (2010) J Phys Chem 132(15):154104
37. Błoński P, López N (2010) J Phys Chem C 116(29):15484–15492
38. Reed AE, Weinstock RB, Weinhold F (1985) J Phys Chem A 83(2): 735–746
39. Dong K, Song Y, Liu X, Cheng W, Yao X, Zhang S (2012) J Phys Chem B 116(3):1007–1017
40. Schwabe T, Grimme S (2007) Phys Chem Chem Phys 9(26):3397–3406
41. Frisch MJ, Trucks GW, Schlegel HB et al (2013) Gaussian 09, revision D.01. Gaussian Inc., Wallingford
42. Speight JG (2005) Lange's handbook of chemistry. McGraw–Hill, New York
43. Clark T, Murray JS, Lane P, Politzer P (2008) J Mol Model 14(8): 689–697
44. Murray JS, Lane P, Politzer P (2008) Int J Quantum Chem 108(15): 2770–2781
45. Lü H, Wang S, Deng C, Ren W, Guo B (2014) J Hazard Mater 279: 220–225
46. Zeng X, Wang H, DeYonker NJ, Mo G, Zhou R, Zhao C (2014) Theor Chem Acc 133:1498–1503